JOURNAL OF GEOPHYSICAL RESEARCH, VOL. 115, A01203, doi:10.1029/2009JA014519, 2010

Phase relations between energetic neutral atom intensities and kilometric radio emissions at Saturn

J. F. Carbary,[1] D. G. Mitchell,[1] S. M. Krimigis,[1] D. A. Gurnett,[2] and W. S. Kurth[2]

Received 1 June 2009; revised 12 October 2009; accepted 15 October 2009; published 13 January 2010.

[1] The intensities of energetic neutral atoms (ENAs) from Saturn's ring current were cross-correlated with Saturn kilometric radiation (SKR, 100–400 kHz) to determine their phase relations. The cross correlations were obtained for three intervals in early 2007 when Cassini was at high northern latitudes and the Ion and Neutral Camera (INCA) could optimally view the entire ring current. During these intervals, the hydrogen, oxygen, and SKR signals all exhibited ~10.8 h periodicities. A consistent phase relation was not observed between the ENA and the SKR. Cross-correlation amplitudes in these intervals varied from 0.25 to 0.79, and the phase offsets varied from ~1 h to several hours and differed according to ENA species. Not only did the SKR and ENA signal show phase offsets, but the H and O signals also displayed offsets. That is, all periodicities at ~10.8 h had no consistent synchronization.

Citation: Carbary, J. F., D. G. Mitchell, S. M. Krimigis, D. A. Gurnett, and W. S. Kurth (2010), Phase relations between energetic neutral atom intensities and kilometric radio emissions at Saturn, *J. Geophys. Res.*, *115*, A01203, doi:10.1029/2009JA014519.

1. Introduction

[2] Saturn's magnetosphere displays a variety of periodicities with the approximate period of ~10.8 h. This period has been recognized in the magnetic field [*Espinosa and Dougherty*, 2000; *Giampieri et al.*, 2006], energetic charged particles [*Carbary and Krimigis*, 1982; *Carbary et al.*, 2007], low-energy particles [*Gurnett et al.*, 2007; *Arridge et al.*, 2008], energetic neutral atoms [*Paranicas et al.*, 2005; *Carbary et al.*, 2008a], and kilometric radiation [*Desch and Kaiser*, 1981; *Kurth et al.*, 2007, 2008]. Periodic oscillations near 10.8 h have also been observed in motions of Saturn's auroral oval and its plasma sheet [*Nichols et al.*, 2008; *Carbary et al.*, 2008b]. Saturn's "clock," however, is not regular but varies over long time intervals on the order of years. The radio period has changed by ~1% on time scales of ~1 year [*Galopeau and Lecacheux*, 2000; *Gurnett et al.*, 2005], and the charged particles and energetic neutrals also show signs of changes in period on time scales of years [*Carbary et al.*, 2009]. The radio periodicities are also modulated by solar wind speed on time scales of 20–30 days [*Zarka et al.*, 2007].

[3] The phase relations between these periodic and quasi-periodic phenomena have recently become a topic of interest because relative phase lead-lag may indicate a cause-effect relation between the phenomena. In a study of magnetometer observations made from October 2007 to July 2006, the relative phase of periodic oscillations in the equatorial perturbation field drifted slowly relative to the Saturn kilometric radiation (SKR) phase, although the ~75° of drift was within the scatter of the SKR phases and might be considered a refinement of a common magnetic field–SKR periodicity [*Andrews et al.*, 2008]. A second study, involving high-latitude observations from October 2006 to May 2007, showed that planetary period oscillations were present on open polar field lines and that the phase relation between the high-latitude and equatorial oscillations implied a rotating, longitudinally asymmetric partial ring current [*Provan et al.*, 2009a]. An intriguing third study of magnetic field oscillations during the 2007 and 2008 Hubble Space Telescope campaign revealed a phase difference of ~180° between the equatorial magnetic field oscillations and auroral oval oscillations; such oscillations would imply an oval displacement within ~35° of the sunward direction at SKR intensity maxima [*Provan et al.*, 2009b].

[4] A close connection is thought to exist between radio emissions and energetic neutral atom (ENA) emissions [*Mitchell et al.*, 2005, 2009], so determining the phase relation between ENA and SKR would be a natural investigation. This paper performs this investigation using half-hour averages of the ENA and SKR data for three intervals during early 2007: days 72–81, days 89–99, and days 108–114. These intervals were selected because during them, Cassini viewed Saturn's equatorial plane from high northern latitudes (>35°) and could completely survey the ring current and because both ENA and SKR exhibited strong variations with the same period.

2. Instrumentation and Data Set

[5] This investigation utilizes observations from two Cassini instruments: the Ion and Neutral Camera (INCA) system of the Magnetospheric Imaging Instrument (MIMI) and the Radio Wave and Plasma Science (RWPS) instrument. The RPWS high-frequency receiver (HFR) detects

[1] Johns Hopkins University Applied Physics Laboratory, Laurel, Maryland, USA.
[2] Department of Physics and Astronomy, University of Iowa, Iowa City, Iowa, USA.

0148-0227/10/2009JA014519$09.00

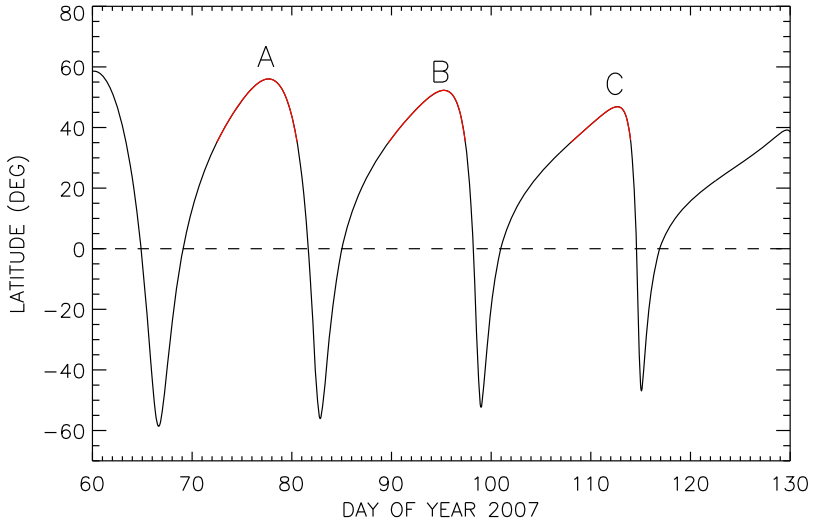

Figure 1. Cassini latitude as a function of time for three orbits in 2007. Red sections of the line indicate intervals when the spacecraft was above 35°N latitude and INCA could view the entire ring current. Intervals A, B, and C were selected for cross-correlation analyses.

electric fields from 3.5 kHz to 16 MHz and measures electric fields in the kilometric band with a spectral resolution of $\Delta f/f \sim 5-20\%$ and a time resolution of <10 s [*Gurnett et al.*, 2004]. Like the Earth's aurora, Saturn's aurora emits radio waves in this wavelength regime of approximately 50–500 kHz [*Kurth et al.*, 2005], with the strongest SKR emissions in the 100–400 kHz regime [*Lamy et al.*, 2008]. Electric field spectral intensities $(V/m)^2\ Hz^{-1}$ from the HFR and other sensors appear in the RPWS key parameter files at a time resolution of 1 min [*Gurnett et al.*, 2004] (see also data obtained from University of Michigan MAPSview Web site http://mapsview.engin.umich.edu). The spectral intensities were first integrated over frequencies between 100 and 400 kHz. The integrated SKR was then averaged within half hour time intervals. Formally, this processing amounts to

$$S = \int_{\Delta t}\int_{\Delta f} (dE/df)dfdt \approx \sum_{\Delta t}\sum_{\Delta f} (dE/df)\delta f\,\delta t,$$

where Δt represents summation over the half-hour time step and Δf represents summation over the SKR frequency range (100–400 kHz). Because S varies over several orders of magnitude, $\log_{10}(S)$ was actually used as the input for cross correlations with ENA. Flagged data (i.e., data having "fill" values of 0.00) were not included in the integrations, and time gaps were also excluded. This processing was conducted for days 1–130 in 2007.

[6] No corrections were made for possible directional effects of the SKR beaming or for $1/r^2$ dependence of the SKR intensity. Visibility of SKR sources is known to depend on observer location, and losses of SKR periodicity during the 130 day interval may have been caused by this effect [*Lamy et al.*, 2008; *Cecconi et al.*, 2009]. A crude range correction may be applied by simply using the spacecraft-Saturn range for r, rather than the (unknown) observer-source range. Application of the spacecraft-Saturn r made little difference in $\log_{10}(S)$, made no difference in the cross correlation phase, and most cases lowered the correlation strengths. However, the $1/r^2$ corrected correlations are included for comparison with the uncorrected correlations in order to judge what effects such a correction might engender. Presumably, correction for either effect would require information about the precise location of the periodic SKR emissions as well as the plasma distribution between the source and Cassini. Such information is not available.

[7] INCA measures energetic neutral atoms with energies between ~3 and >220 keV with a spatial resolution of ~4° × 8° [*Krimigis et al.*, 2004, 2005]. In particular, INCA detects H atoms (20–50 keV) and O atoms (64–144 keV), and these two neutral channels are used herein. Although the time resolution of INCA is ~6 min per image, the ENA data are sufficiently noisy to require averaging into 1/2 h time bins to improve the signal for further analysis. Each average ENA image has 32 × 32 pixels. The mean pointing direction of each pixel is obtained in the SZS coordinate system (Z is along Saturn spin axis, $Y = Z \times S$, where S is the Sun direction, and X completes right-hand system). The pixel directions are projected to their intersections of the XY (equatorial) plane, and the intensities are corrected for slant viewing and the Compton-Getting effect. This projection and INCA processing were detailed in a previous publication [*Carbary et al.*, 2008c].

[8] Cassini must be at sufficiently high latitude to view Saturn's equatorial plane without distortion caused by a high "slant" angle. For the slant path distortion to be less than the point spreading of one pixel, Cassini was required to be at latitudes above ~35°. The slant corrections become progressively less reliable as latitude decreases. The high-latitude conditions prevailed during several orbits in early 2007. Figure 1 indicates the latitude versus time profile for 70 days in 2007. The red sections of the line indicate three intervals when Cassini's latitude exceeded 35° and INCA could competently observe the ring current from above. Each interval lasted several days and afforded the opportunity to measure ENA quasi-continuously.

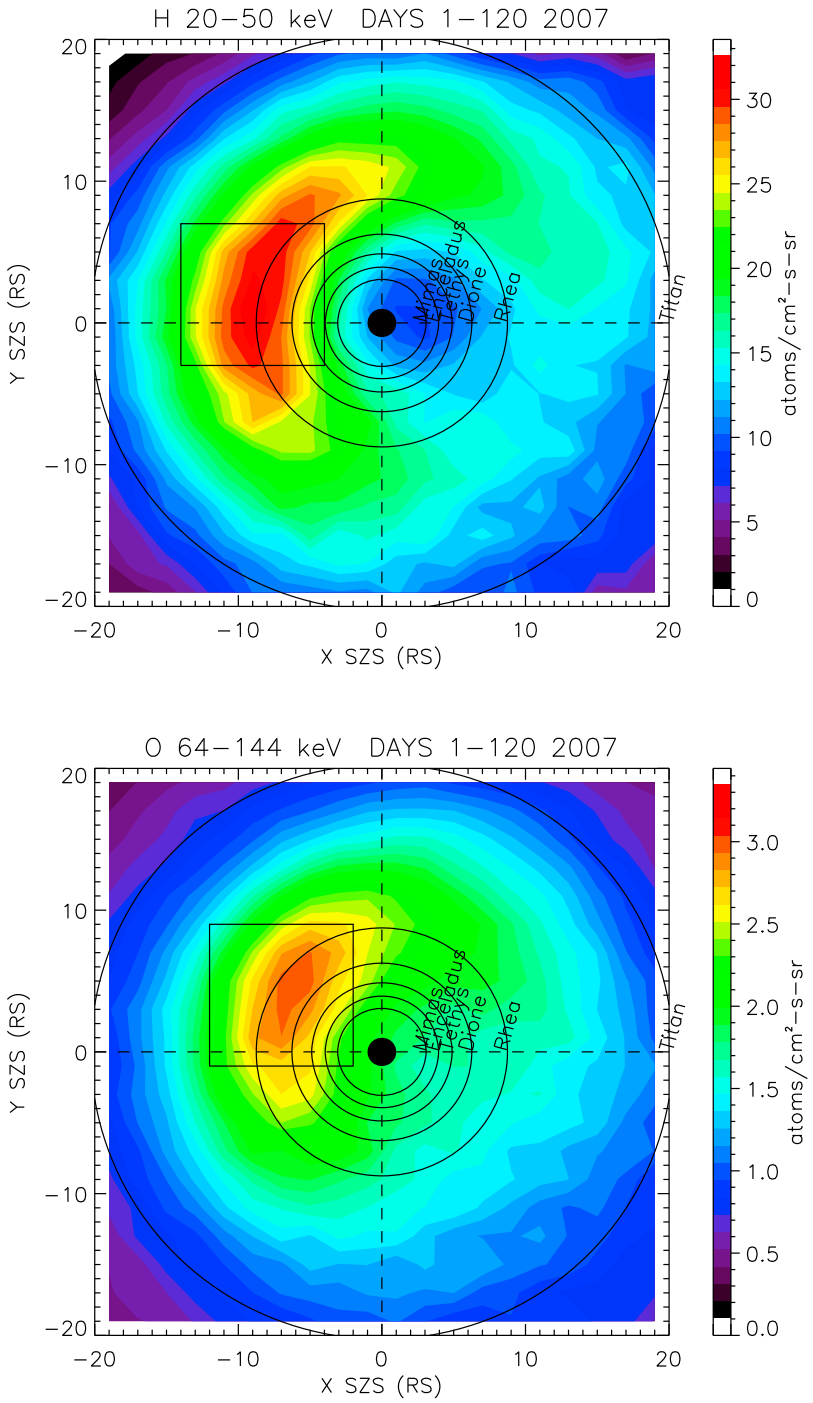

Figure 2. Composite images, projected onto the SZS equatorial plane, of energetic (top) hydrogen and (bottom) oxygen emissions. The images represent averages of ENA intensities in 2×2 R_S bins from days 1–120 (2007) when Cassini was at latitudes exceeding 35°N. The x axis points sunward, and the y axis points toward dusk. Square boxes 10×10 R_S enclose the most intense ENA emissions of both species. Averages of intensities within these boxes were calculated as a function of time and compared to SKR time profiles.

[9] Favorable, high-latitude viewing persisted for the first ~130 days of 2007. However, periodic behavior in both the ENA and SKR signals occurred only during the three intervals cited here. The periodic SKR signal may have vanished because of changing geometry between the observer and source [*Lamy et al.*, 2008]. Alternately, either the ENA or the SKR oscillation might have become attenuated because of some variation in a possible external driver, such as solar wind speed [*Zarka et al.*, 2007]. For purposes of phase measurement, this study considered

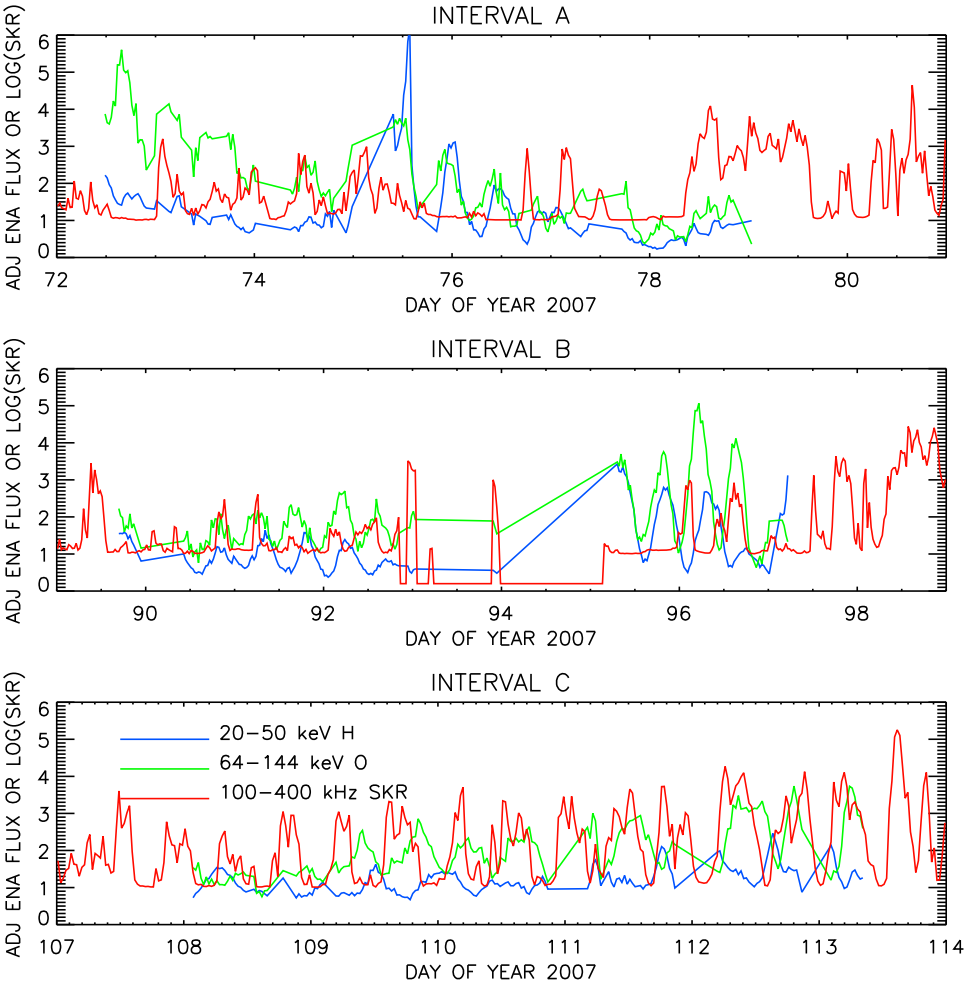

Figure 3. Box averages of energetic hydrogens (blue lines) and oxygens (green lines) compared to SKR averages (red lines) for the three intervals in Figure 1. In each case, the data have been averaged in time to 1/2 h resolution.

only times when both the ENA and SKR signals presented oscillations with the same period.

3. Periodicity in the Three Intervals

[10] A composite image of all of the high-latitude ENA data provides an instructive introduction to INCA processing. Figure 2 displays just such composites of energetic hydrogen and oxygen atoms for the first 120 days of 2007, including the three study intervals, days 71–81 (interval A), days 89–99 (interval B), and days 107–144 (interval C). The composites were formed by averaging all of the 1/2 h imagery into 2 R_S × 2 R_S bins in SZS XY coordinates for times when the spacecraft latitude exceeded 35°N. The strongest ENA emissions show up on the night side of Saturn, approximately between the orbits of Dione and Rhea, and have maxima in the premidnight section [*Carbary et al.*, 2008c]. The peak H emission appears at approximately $X = -9R_S$ and $Y = 2R_S$, while the peak O emission is at $X = -7R_S$ and $Y = 4R_S$.

[11] Time profiles of ENA emissions are constructed by averaging the intensities within $10R_S \times 10R_S$ boxes centered on the peak locations noted above. The box averaging is performed for each 1/2 h ENA image from the high-latitude observations. The same periods would be realized for different box locations; selection of averages from the maximum intensity boxes ensures the best statistics from those regions thought to be associated with particle acceleration in Saturn's magnetosphere [*Carbary et al.*, 2008c].

[12] Figure 3 shows time profiles from this box-averaging process applied to the three study intervals. The hydrogen and oxygen time profiles (blue and green lines) are compared to the SKR averages (red line) at the same time resolution. Although gaps exist, periodic signals can be recognized in all the profiles. Figure 4 reveals the approximate periods for each signal in each interval. The periods are seen as the peaks in the Lomb periodograms derived from each time profile [e.g., *Carbary et al.*, 2007]. The signals for each interval share a common period. Intervals A and B have common periods of ~10.8 h, while interval C exhibits a common period of ~10.6 h. Both the 10.8 and 10.6 h periods have been recognized as distinct SKR periods [*Kurth et al.*, 2008; *Gurnett et al.*, 2009]. Since the periods are the same, a definite phase relation

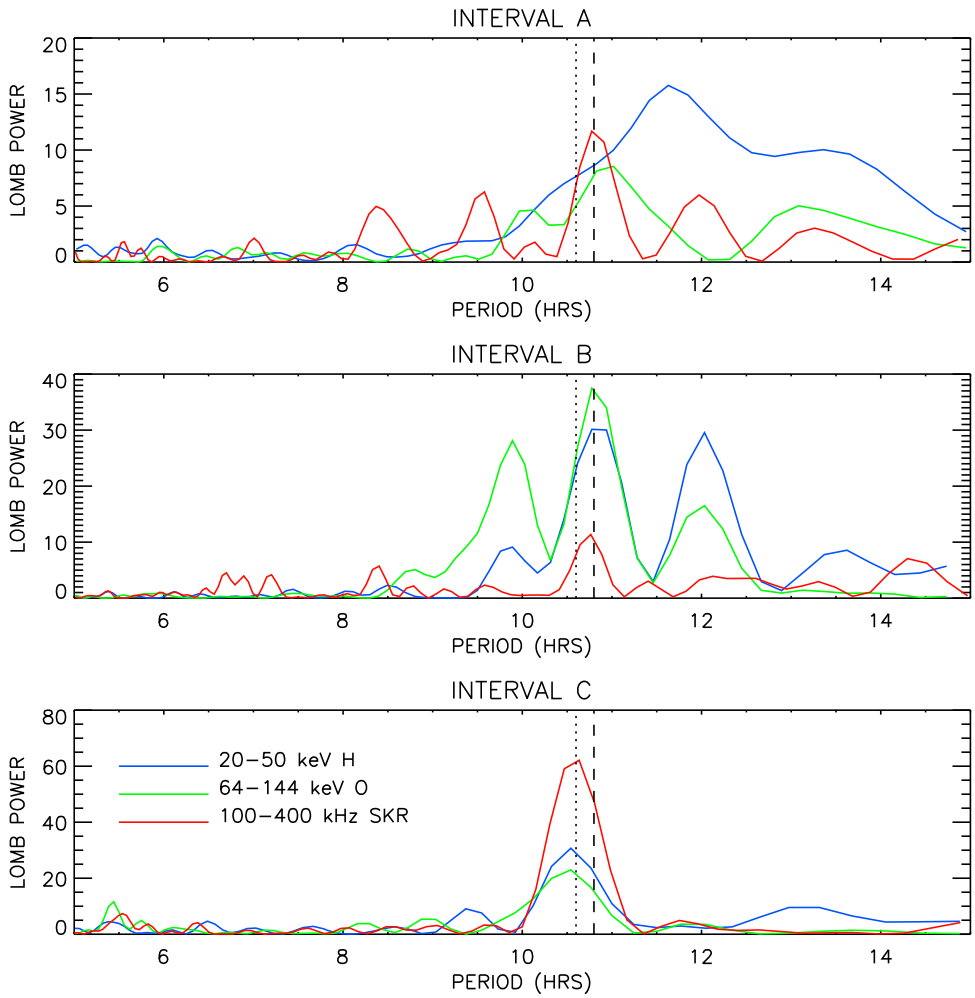

Figure 4. Lomb spectrograms of neutral hydrogen (blue lines), neutral oxygen (green lines), and SKR (red lines) for the three intervals of Figure 1. The dashed line indicates a 10.8 h period, while the dotted line indicates a 10.6 h period.

should exist between the signals. This phase relation can be quantified by performing a simple cross-correlation analysis.

4. Cross Correlations in the Three Intervals

[13] Before proceeding, a short discussion of the cross correlation is in order. Cross correlation consists of sliding in time one signal relative to another and then comparing the signals. The optimum time offset (amount of sliding) is judged by some correlative measure such as the linear correlation or rank order. The various types of correlation are discussed by *Press et al.* [1992]. The present analysis employs simple linear (Pearson) correlation; use of rank correlation (Kendall or Spearman) was performed but gave essentially the same results. The cross correlations were implemented on the discrete, half hour signals (Figure 2) using the Interactive Data Language (IDL) C_CORRELATE function. (As noted previously, the ENA signal is a box average of a spatial region, while the SKR signal is the logarithm of the frequency-integrated intensity.) The cross-correlation window (or amount of time sliding) was 100 half-hour increments or ±25 h. The window extended well beyond the ~10.8 h signal period in order to capture possible effects extending beyond one cycle. The "best" correlation between signals is judged by the peak in the linear correlation coefficient as a function of offset time. The uncertainty in the peak is ±1 increment or ±1/2 h.

[14] Figure 5 displays the cross correlations between all three signals (H, O, and SKR) for each of the three intervals. The blue and green traces show the H and O neutral atom correlations with the SKR, while the red traces show the H correlation with O. The latter correlation was included to show possible phase differences between the ENA signals themselves. The dashed lines indicate ENA-SKR correlations for which a $1/r^2$ correction was applied to the SKR signal, while solid lines show correlations made with uncorrected signals.

[15] Figure 5 (top) shows cross correlations for the first interval, days 72–80 of 2007. Both ENA × SKR signals had a peak cross correlation of ~0.40, with the offset peak at +11.5 h. This peak is just outside the cycle window of 10.8 h. That is, if the H and O signals are advanced 11.5 h relative to the SKR signal, they will, for this case, achieve a maximum correlation with the SKR. The cross correlation between the H and O signals achieves a maximum of ~0.56

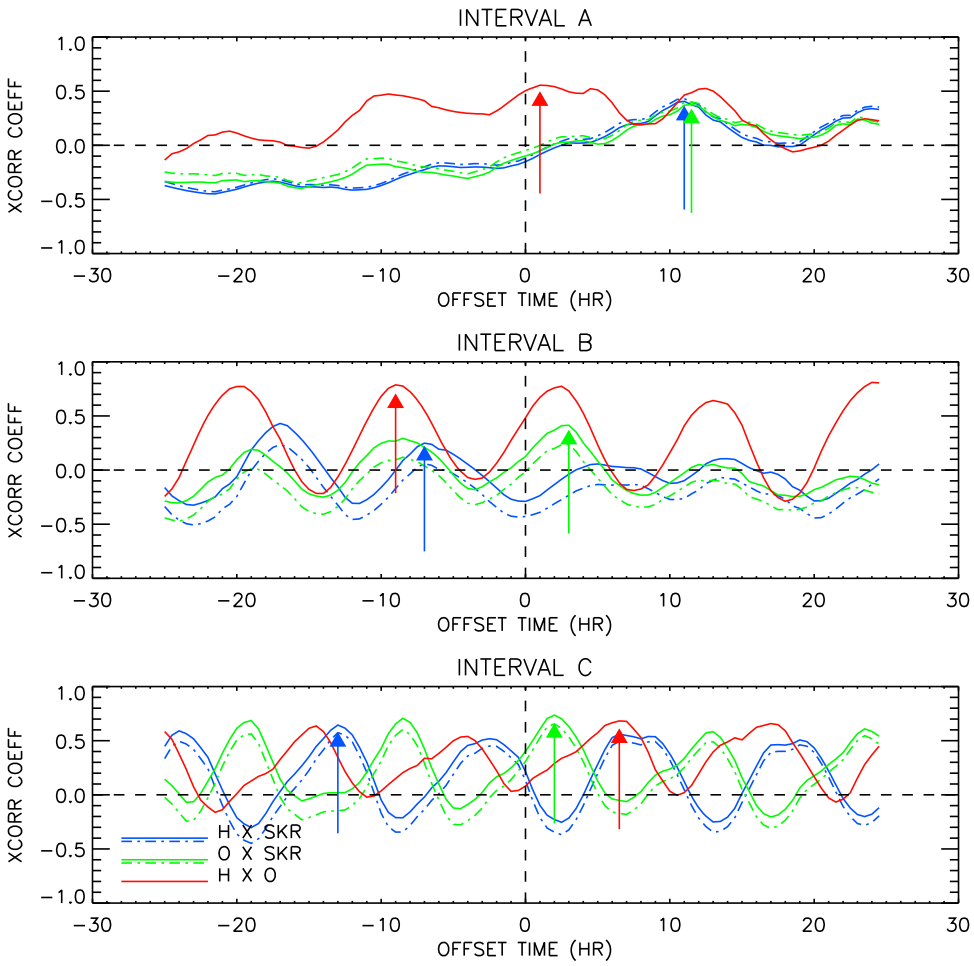

Figure 5. Cross correlation between SKR and energetic hydrogen atoms (blue lines) and energetic oxygens (green lines) for the three time intervals. Negative offset times indicate the ENA signal lags the SKR signal, while positive times indicate the ENA signal leads the SKR signal. The red traces indicate the cross correlation between energetic hydrogen and energetic oxygen. Blue, green, and red arrows mark maxima in the respective traces. Solid blue and green lines indicate ENA-SKR correlations without the application of a $1/r^2$ correction to the SKR signal, while dashed blue and green lines show correlations for which a $1/r^2$ correction was applied.

at +1 h, which suggests that the two signals are approximately in phase, as one might expect. The H × O cross correlation also displays an approximately sinusoidal shape. This shape is characteristic of two sinusoidally varying signals, as shown in section 5.

[16] Figure 5 (middle) displays the cross correlations for the second interval, days 89–98 of 2007. Distinctly different cross correlations appear for the ENA × SKR signals in this interval. Within the ±10.8 h cycle window, the H × SKR cross correlation maximizes at −7.0 h with only a weak coefficient of 0.25. However, a somewhat stronger correlation appears between H and SKR at an offset time of −17.0 h. The sinusoidal shape of this correlation suggests a phase difference of approximately $-7.0 \pm N \times 10.8$ h (where N is an integer). The O × SKR cross correlation has a higher peak of 0.41 at +3 h and also has a sinusoidal shape. Thus, the H × SKR and O × SKR cross correlations differ significantly during this interval. They also differ dramatically from those of the first interval. Finally, the red trace for the H × O cross correlation achieves a maximum of 0.79 at −9.0 h, or $-9.0 \pm N \times 10.8$ h. This phase difference is similar to but not identical to that of the first interval.

[17] Figure 5 (bottom) exhibits the cross correlations from days 107–144 of 2007. These are the strongest cross correlations of this investigation. All cross correlations are sinusoidal, and all have coefficient peaks exceeding 0.6, which indicates very good correlations at the particular phase offsets. The H × SKR cross correlation maximizes at $-13.0 \pm N \times 10.8$ h, which differs from the O × SKR maximum of 0.74 at $2.0 \pm N \times 10.8$ h. Peaking at $6.5 \pm N \times 10.8$ h, the H × O cross correlation differs from both of the SKR cross correlations. Furthermore, all of these cross correlations of interval C differ from those of the preceding intervals, suggesting the phases between all periodic signals have not remained constant for more than a few weeks.

[18] Table 1 summarizes the cross correlation results for the three intervals. The offset time in hours of the peak cross correlation between the two signals are indicated. The numb-

Table 1. Cross Correlation Results for Three Intervals in 2007[a]

Interval	Days of Interval in 2007	H × SKR	O × SKR	H × O
A	72–80	+11.0 (0.41)	11.5 (0.38)	1.0 (0.56)
B	90–98	−7.0 (0.25)	+3.0 (0.41)	−9.0 (0.79)
C	107–113	−13.0 (0.64)	+2.0 (0.74)	+6.5 (0.68)

[a]Uncorrected SKR signals only. Each entry represents the offset time in hours of the peak cross correlation between the two signals indicated; strength of the correlation r^2, ranging from 0.0 (no correlation) to 1.0 (perfect correlation), is given in parentheses.

ers in parentheses represent the strength of the correlation (0.0 being no correlation and 1.0 being perfect correlation).

5. Simulation

[19] A simple simulation involving two periodic signals will help explain the observed cross correlations. Assume the signals have the same period T(=10.8 h) so they have the same angular frequency $\omega = 2\pi/T$ and a phase difference of t_1 hours. The two signals S_1 and S_2 can be represented as

$$S_1(t) = A_1 \sin[\omega(t - t_1)] + \eta(t)$$

$$S_2(t) = A_2 \sin[\omega t] + \delta(t),$$

where A_1 and A_2 are the amplitudes of the signals, and $\eta(t)$ and $\delta(t)$ are random noise fluctuations. The noise can be quite significant (up to 75% of signal here), and valid cross correlations can still be found between S_1 and S_2. Here, A_1 = 1.0, A_2 = 0.5, and t_1 = 3 h. As in the observation, the time resolution is 1/2 h.

[20] Figure 6 shows the two simulated signals and their cross correlation. The cross correlation has a peak at the expected offset times of 3 ± 10.8 h. The cross correlation exhibits a distinctive sinusoidal pattern very similar to that seen in the actual cross correlations of Figure 5. This similarity suggests the double-sinusoid model does not differ greatly from the observational case. The simulation also shows that cross correlation of two rather noisy signals of differing amplitudes can yield an accurate measure of the phase offset of the signals.

6. Discussion

[21] Both observations and simulations suggest that the H, O, and SKR periodicities can be approximated by noisy sinusoids with different phase offsets. The phase offsets should not be construed as indicative of a causal relation between ENA and SKR. That is, a phase lag of 3 hours in ENA flux relative to SKR does not necessarily mean the SKR (or the plasma instabilities initiating the radio emis-

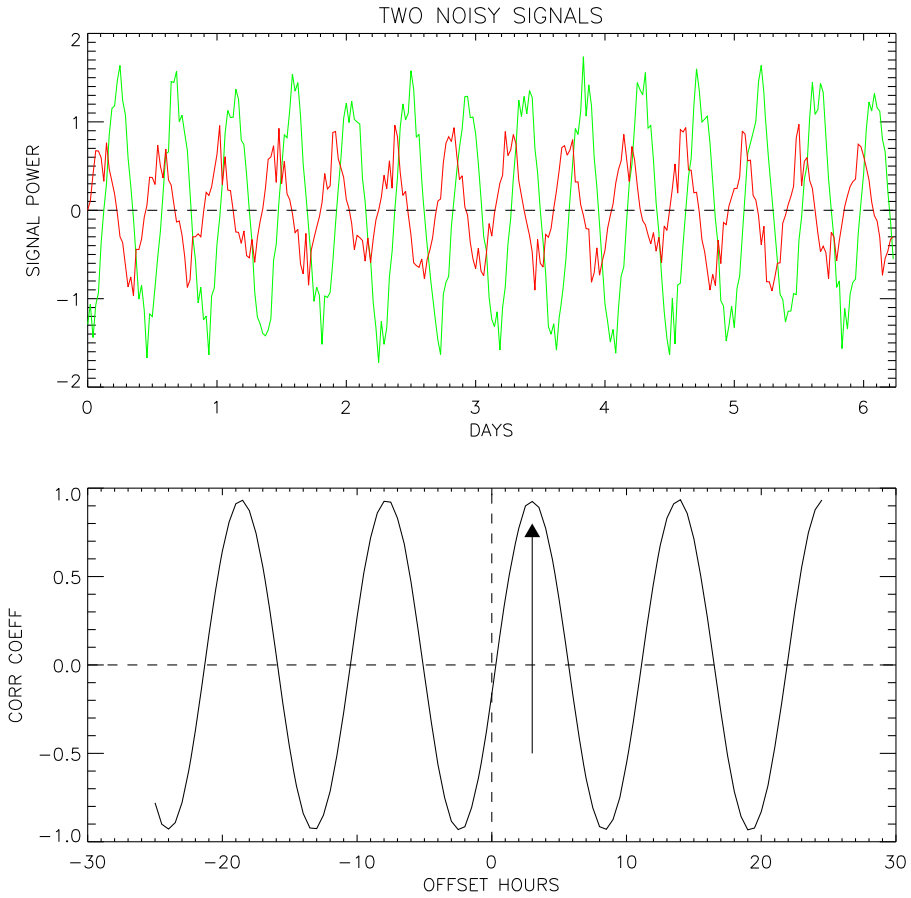

Figure 6. (top) Simulation of two signals and (bottom) their cross correlation. In Figure 6 (top) S_1 (green line) is a sine wave with different phase and amplitude than S_2 (red line). Random noise has been added to each signal. Figure 6 (bottom) indicates the simulated cross correlation, showing a peak at ~3 h, which is identical to the phase difference of S_1 relative to S_2.

sions) somehow generate ENA emissions 3 hours later. Rather, the phase differences show that although the ENA and SKR "clocks" run at about the same rate and keep the same "time," they have different zero points. By analogy, a clock in New York runs at the same rate as a clock in San Francisco, but the two differ in phase by three hours.

[22] Unlike the New York–San Francisco phase difference, however, the phase differences in the three clocks also changed over the several weeks of the observation interval. This time scale is similar to that over which the solar wind speed modulates SKR periodicities [*Zarka et al.*, 2007]. Possibly, pressure pulses in the solar wind may act to "reset" the ENA clock, which would affect the ENA-SKR relative phases. How solar wind variations affect the ENA or ENA × SKR cross correlations will be a future topic for investigation when more solar wind data become available.

[23] Strangely, the H and O signals were not always in phase, nor did they maintain a consistent phase. This behavior suggests that the hydrogen and oxygen clocks are reset by different mechanisms. Both species of neutrals are generated by charge exchange collisions between low-energy H and O neutrals and energetic protons and oxygen ions. The distribution of low-energy neutrals is thought to be nonperiodic, although it is "lumpy" [e.g., *Shemansky and Hall*, 1992], so any ENA periodicity must be ascribed to the energetic ions. The energetic ions do exhibit ~10.8 h periodicity, but their phase relations are (as yet) unknown [*Carbary et al.*, 2007]. Energetic ion fluxes do seem to vary in phase when plotted as functions of time. Resetting the H or O periodicity may involve sudden, sporadic changes in the neutral gas at Saturn. A natural way to do this would be through sudden, sporadic changes in the neutral gas source, namely, the outgassing of the plumes of Enceladus [*Porco et al.*, 2006].

[24] One final caveat should be noted. The ENA signals represent the maximum intensities observed in the premidnight sector where intensity maxima are statistically observed [*Carbary et al.*, 2008c]. The current investigation assumes that signals from this region are representative of the ENA periodicities. There exists no a priori reason why this region should be "more" periodic or "less" periodic than other local time regions, but such could be the case. After all, the SKR periodicities are associated with the dawn to noon sectors of the magnetosphere [e.g., *Cecconi et al.*, 2009], so another place to derive the ENA signal might be local times from 0600 to 1200. Several detailed case studies have shown that ENA, SKR, and the aurora all brighten in the midnight to dawn sector, and such signatures may represent recurrent energization of plasma [*Mitchell et al.*, 2009]. Another strategy might be to sum the intensity of the entire ring current (i.e., sum over all local times) and correlate the sum with SKR. Whole-image summing has been used before and does exhibit periodicity [*Paranicas et al.*, 2005]. The premidnight sector was chosen here to represent the ENA emissions merely because it showed the highest ENA intensities, which should be expected to offer the highest signals.

7. Conclusions

[25] ENA intensities from Saturn's ring current were cross-correlated with Saturn kilometric radiation for three intervals in early 2007 when Cassini was at latitudes above 35°N and could view the equatorial plane. The cross-correlation strengths and phase offsets between the ENA and SKR varied considerably, and a definite phase between the ENA and SKR signals did not exist. Even cross correlations between the two ENA species, hydrogen and oxygen, apparently changed. The phases between signals did not remain consistent for longer than a few days at a time.

[26] **Acknowledgments.** This research was supported in part by the NASA Office of Space Science under task order 003 of contract NAS5–97271 between NASA Goddard Space Flight Center and Johns Hopkins University and in part by NASA grant NNH06ZDA001N from the Cassini Data Analysis Program (CDAP). The research at the University of Iowa was supported by NASA through contract 1356500 through the Jet Propulsion Laboratory.

[27] Wolfgang Baumjohann thanks the reviewers for their assistance in evaluating this paper.

References

Andrews, D. J., E. J. Bunce, S. W. H. Cowley, M. K. Dougherty, G. Provan, and D. J. Southwood (2008), Planetary period oscillations in Saturn's magnetosphere: Phase relation of equatorial magnetic field oscillations and Saturn kilometric radiation modulation, *J. Geophys. Res.*, *113*, A09205, doi:10.1029/2007JA012937.

Arridge, C. S., N. André, N. Achilleos, K. K. Khurana, C. L. Bertucci, L. K. Gilbert, G. R. Lewis, A. J. Coates, and M. K. Dougherty (2008), Thermal electron periodicities at 20 R_S in Saturn's magnetosphere, *Geophys. Res. Lett.*, *35*, L15107, doi:10.1029/2008GL034132.

Carbary, J. F., and S. M. Krimigis (1982), Charged particle periodicity in the Saturnian magnetosphere, *Geophys. Res. Lett.*, *9*, 1073–1076, doi:10.1029/GL009i009p01073.

Carbary, J. F., D. G. Mitchell, S. M. Krimigis, D. C. Hamilton, and N. Krupp (2007), Charged particle periodicities in Saturn's outer magnetosphere, *J. Geophys. Res.*, *112*, A06246, doi:10.1029/2007JA012351.

Carbary, J. F., D. G. Mitchell, P. Brandt, C. Paranicas, and S. M. Krimigis (2008a), ENA periodicities at Saturn, *Geophys. Res. Lett.*, *35*, L07102, doi:10.1029/2008GL033230.

Carbary, J. F., D. G. Mitchell, P. Brandt, E. C. Roelof, and S. M. Krimigis (2008b), Periodic tilting of Saturn's plasma sheet, *Geophys. Res. Lett.*, *35*, L24101, doi:10.1029/2008GL036339.

Carbary, J. F., D. G. Mitchell, P. Brandt, E. C. Roelof, and S. M. Krimigis (2008c), Statistical morphology of ENA emissions at Saturn, *J. Geophys. Res.*, *113*, A05210, doi:10.1029/2007JA012873.

Carbary, J. F., S. M. Krimigis, D. G. Mitchell, C. Paranicas, and P. Brandt (2009), Energetic neutral atom (ENA) and charged particle periodicities in Saturn's magnetosphere, *Adv. Space Res.*, *44*(4), 483–493, doi:10.1016/j.asr.2009.04.019.

Cecconi, B., L. Lamy, P. Zarka, R. Pangé, W. S. Kurth, and P. Louarn (2009), Goniopolarimetric study of the revolution of 29 perikrone using the Cassini Radio and Plasma Wave Science Instrument high-frequency receiver, *J. Geophys. Res.*, *114*, A03215, doi:10.1029/2008JA013830.

Desch, M. D., and M. L. Kaiser (1981), Voyager measurements of the rotation period of Saturn's magnetic field, *Geophys. Res. Lett.*, *8*, 253–256, doi:10.1029/GL008i003p00253.

Espinosa, S. A., and M. K. Dougherty (2000), Periodic perturbations in Saturn's magnetic field, *Geophys. Res. Lett.*, *27*, 2785–2788, doi:10.1029/2000GL000048.

Galopeau, P. H. M., and A. Lecacheux (2000), Variations in Saturn's radio rotation period measured at kilometer wavelengths, *J. Geophys. Res.*, *105*, 13,089–13,101, doi:10.1029/1999JA005089.

Giampieri, G., M. K. Dougherty, E. J. Smith, and C. T. Russell (2006), A regular period for Saturn's magnetic field that may track its internal rotation, *Nature*, *441*, 62–64, doi:10.1038/nature04750.

Gurnett, D. A., et al. (2004), The Cassini radio and plasma wave investigation, *Space Sci. Rev.*, *114*, 395–463, doi:10.1007/s11214-004-1434-0.

Gurnett, D. A., et al. (2005), Radio and plasma wave observations at Saturn from Cassini's approach and first orbit, *Science*, *307*, 1255–1259, doi:10.1126/science.1105356.

Gurnett, D. A., A. M. Persoon, W. S. Kurth, J. B. Groene, T. F. Averkamp, M. K. Dougherty, and D. J. Southwood (2007), The variable rotation period of the inner region of Saturn's plasma disk, *Science*, *316*, 442–445, doi:10.1126/science.1138562.

Gurnett, D. A., A. Lecacheux, W. S. Kurth, A. M. Persoon, J. B. Groene, L. Lamy, P. Zarka, and J. F. Carbary (2009), Discovery of a north-south asymmetry in Saturn's radio rotation period, *Geophys. Res. Lett.*, *36*, L16102, doi:10.1029/2009GL039621.

Krimigis, S. M., et al. (2004), Magnetospheric Imaging Instrument (MIMI) on the Cassini mission to Saturn/Titan, *Space Sci. Rev.*, *114*, 233–329, doi:10.1007/s11214-004-1410-8.

Krimigis, S. M., et al. (2005), Dynamics of Saturn's magnetosphere from MIMI during Cassini's orbital insertion, *Science*, *307*, 1270–1273, doi:10.1126/science.1105978.

Kurth, W. S., et al. (2005), An Earth-like correspondence between Saturn's auroral features and radio emission, *Nature*, *433*, 722–725, doi:10.1038/nature03334.

Kurth, W. S., A. Lecacheux, T. F. Averkamp, J. B. Groene, and D. A. Gurnett (2007), A Saturnian longitude system based on a variable kilometric radiation period, *Geophys. Res. Lett.*, *34*, L02201, doi:10.1029/2006GL028336.

Kurth, W. S., T. F. Averkamp, D. A. Gurnett, J. B. Groene, and A. Lecacheux (2008), An update to a Saturnian longitude system based on kilometric radio emissions, *J. Geophys. Res.*, *113*, A05222, doi:10.1029/2007JA012861.

Lamy, L., P. Zarka, B. Cecconi, R. Prangé, W. S. Kurth, and D. A. Gurnett (2008), Saturn kilometric radiation: Average and statistical properties, *J. Geophys. Res.*, *113*, A07201, doi:10.1029/2007JA012900.

Mitchell, D. G., et al. (2005), Energetic ion acceleration in Saturn's magnetosphere: Substorms at Saturn?, *Geophys. Res. Lett.*, *32*, L20S01, doi:10.1029/2005GL022647.

Mitchell, D. G., et al. (2009), Recurrent energization of plasma in the midnight-to-dawn quadrant of Saturn's magnetosphere, and its relationship to auroral UV and radio emissions, *Planet. Space Sci.*, *57*, 1732–1742, doi:10.1016/j.pss.2009.04.002.

Nichols, J. D., J. T. Clarke, S. W. H. Cowley, J. Duval, A. J. Farmer, J.-C. Gérard, D. Grodent, and S. Wannawichian (2008), Oscillation of Saturn's southern auroral oval, *J. Geophys. Res.*, *113*, A11205, doi:10.1029/2008JA013444.

Paranicas, C., D. G. Mitchell, E. C. Roelof, P. C. Brandt, D. J. Williams, S. M. Krimigis, and B. H. Mauk (2005), Periodic intensity variations in global ENA images, *Geophys. Res. Lett.*, *32*, L21101, doi:10.1029/2005GL023656.

Porco, C. C., et al. (2006), Cassini observes active south pole of Enceladus, *Science*, *311*, 1393–1401, doi:10.1126/science.1123013.

Press, W. H., S. A. Teukolsky, W. T. Vetterling, and B. P. Flannery (1992), *Numerical Recipes in FORTRAN: The Art of Scientific Computing*, 2nd ed., chap. 13.8, pp. 569–577, Cambridge Univ. Press, Cambridge, U. K.

Provan, G., D. J. Andrews, C. S. Arridge, A. J. Coates, S. W. H. Cowley, S. E. Milan, M. K. Dougherty, and D. M. Wright (2009a), Polarization and phase of planetary-period magnetic field oscillations on high-latitude field lines in Saturn's magnetosphere, *J. Geophys. Res.*, *114*, A02225, doi:10.1029/2008JA013782.

Provan, G., S. W. H. Cowley, and J. D. Nichols (2009b), Phase relation of oscillations near the planetary period of Saturn's auroral oval and the equatorial magnetospheric magnetic field, *J. Geophys. Res.*, *114*, A04205, doi:10.1029/2008JA013988.

Shemansky, D. E., and D. T. Hall (1992), The distribution of neutral hydrogen in the magnetosphere of Saturn, *J. Geophys. Res.*, *97*(A4), 4143–4161, doi:10.1029/91JA02805.

Zarka, P., L. Lamy, B. Cecconi, and R. Prangé (2007), Modulation of Saturn's radio clock by solar wind speed, *Nature*, *450*, 265–267, doi:10.1038/nature06237.

J. F. Carbary, S. M. Krimigis, and D. G. Mitchell, Johns Hopkins University Applied Physics Laboratory, 11100 Johns Hopkins Rd., Laurel, MD 20723, USA. (james.carbary@jhuapl.edu)

D. A. Gurnett and W. S. Kurth, Department of Physics and Astronomy, University of Iowa, Iowa City, IA 52242, USA.